Rapid Communications | Editors' Suggestion

Probing short-range magnetic order in a geometrically frustrated magnet by means of the spin Seebeck effect

Changjiang Liu,[1] Stephen M. Wu,[1,2] John E. Pearson,[1] J. Samuel Jiang,[1] N. d' Ambrumenil,[3] and Anand Bhattacharya[1,*]

[1]*Materials Science Division, Argonne National Laboratory, Lemont, Illinois 60439, USA*

[2]*Department of Electrical and Computer Engineering, University of Rochester, Rochester, New York 14627, USA*

[3]*Department of Physics, University of Warwick, Coventry CV4 7AL, United Kingdom*

(Received 29 March 2018; published 28 August 2018)

The spin Seebeck effect (SSE) is a phenomenon where a spin current is generated from thermal excitations in magnetic materials. It is believed that magnetic long-range order (LRO) is not required for SSE, while short-ranged order (SRO) plays an important role. However, a definitive experimental demonstration of the connection between the SSE and SRO has been missing. Here, we show that the SSE is able to probe a specific SRO in a model geometrically frustrated magnet $Gd_3Ga_5O_{12}$ (GGG). A field-induced SRO in GGG is detected by the SSE in the temperature range 2–5 K. The origin of the SRO is verified by comparing the SSE data directly to existing neutron scattering measurements at much lower temperatures ($T < 0.9$ K), where field-induced LRO exists. Our theoretical calculations of the magnetic structure further confirm the anisotropic field dependence of the SRO in GGG. These findings establish that the SSE can serve as an effective probe of SRO in geometrically frustrated magnets.

DOI: 10.1103/PhysRevB.98.060415

Pure spin currents carried by magnetic excitations are of fundamental interest and may be used to transmit and store information [1]. One method of generating a pure spin current is through the spin Seebeck effect (SSE), where a thermal gradient drives a current of magnons. Spin currents have been generated in this way by using both ferromagnetic (FM) [2] and antiferromagnetic (AFM) [3,4] magnons. It has been shown that even for correlated paramagnetic insulators, a spin current may be generated via the SSE or paramagnetic spin pumping [5–7]. It is presumed that this is due to short-lived magnons (paramagnons) arising as a result of short-range correlations between spins [5,8–11].

Current understanding of the SSE in magnetic insulators is based on the diffusion of thermally excited magnons [12–15]. Such a mechanism is supported by recent experiments studying the length scale, temperature, and magnetic field dependencies of SSE in ferrimagnetic insulator yttrium iron garnet (YIG) [16–18]. Diffusive magnons have a finite lifetime and diffusion length. The fact that the SSE can be measured in nanometer thickness YIG films and on picosecond timescales [19] suggests that the SSE is sensitive to magnons in very small volumes or with very short lifetimes. These properties of SSE suggest that it may be used as a sensitive probe of magnetic short-range order (SRO). In fact, evidence for this has been mounting in the spintronics community [5,7], though an explicit demonstration of the relationship between the SSE and SRO has yet to be reported.

In this Rapid Communication, we explore the link between the SSE and SRO by performing the experiment on a canonical geometrically frustrated magnet gadolinium gallium garnet ($Gd_3Ga_5O_{12}$, GGG), which is also believed to be a classical spin liquid [20–22]. One of the distinguishing features of geometrically frustrated magnets is that at temperatures well below the scale set by the exchange interactions ($\theta_{CW} = -2.3$ K in GGG), the spins become strongly correlated but there is an absence of LRO. In this regime, SRO is assumed to play an important role. In our measurements on GGG, we find significant magnetic-field-induced modulations in the spin current generated by the SSE in the temperature range 2–5 K, close to $|\theta_{CW}|$. Furthermore, we find that these modulations follow the field dependence of a particular antiferromagnetic peak measured by neutron diffraction at much lower temperatures, where LRO is observed. This finding represents an explicit demonstration of the connection between the SSE and SRO. Importantly, neutron scattering measurements cannot resolve the magnetic-field-induced SRO at temperatures of $T = 1.3$ K and above, suggesting that the SSE is a very sensitive probe of SRO. Additionally, at higher fields up to 90 kOe, our SSE measurements show extra structure, hinting at the existence of further field-induced spin dynamics.

As shown in Fig. 1(a), the Gd sites in GGG form a hyperkagome lattice, a three-dimensional kagome lattice consisting of two interpenetrating corner-sharing triangular sublattices [23,24]. The exchange interactions between nearest-neighbor Gd^{3+} ions are antiferromagnetic. Owing to geometrical frustration, GGG hosts a rich magnetic phase diagram at low temperatures ($T < 1$ K) [24]. At zero magnetic field, there is no magnetic LRO in GGG down to 25 mK, far below $|\theta_{CW}| = 2.3$ K [6,23,25,26]. It has been shown that many fundamentally interesting phases arise within GGG, including spin-liquid states [23], protected spin clusters [27], and a hidden multipolar order [22].

In our experiments, we perform SSE measurements on GGG in the temperature regime (2–5 K) where effects due to geometric frustration become stronger as we approach $|\theta_{CW}|$. SSE devices were patterned onto GGG single crystals with a polished surface along (111) or (001). Platinum (Pt) was

*anand@anl.gov

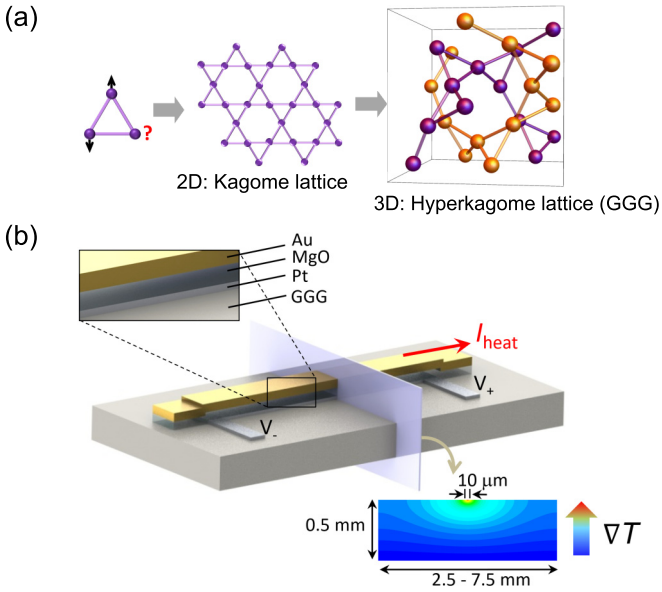

FIG. 1. GGG hyperkagome lattice and schematics of the SSE device. (a) Illustration of geometrical frustration of antiferromagnetically coupled spins on a triangular lattice. The kagome lattice is a realization of such frustration in two-dimensional space. When extended to three dimensions, corner-sharing triangles form the hyperkagome lattice. For GGG, the two interpenetrating corner-sharing triangular sublattices are shown in purple and orange, respectively. (b) Device design of an on-chip heated SSE device. The upper left panel shows the vertical structure of the fabricated device. A cross-sectional view of the simulated temperature profile in GGG is shown in the bottom panel.

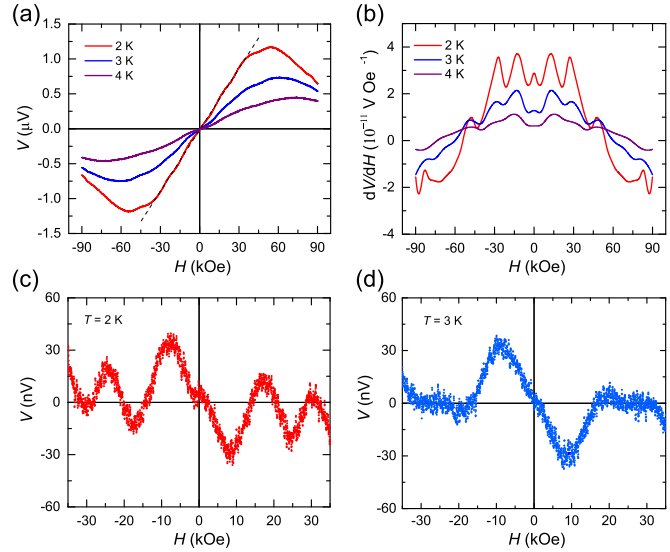

FIG. 2. SSE measurement results and modulations in the SSE response. (a) SSE measurement results at temperatures below 5 K with magnetic field applied along the [100] crystal axis. (b) Derivative of SSE voltage with respect to magnetic field (dV/dH) showing extra field-dependent modulations in the SSE signal. (c), (d) Modulations in the SSE voltage plotted directly in the field range -35 kOe $< H <$ 35 kOe after subtracting a linear background from the SSE signal at $T = 2$ and 3 K, respectively.

used as the spin detector material. Local heating was achieved by passing an electric current through a gold heater wire, electrically isolated from the spin detector layer by a thin MgO layer. The typical heater power used in our experiment is 0.16 mW, which raises the temperature near the surface of GGG. Using the resistance of the Pt wire for thermometry and the thermal conductivity values of GGG at low temperatures [28], we estimate that the increase in surface temperature is $\Delta T \sim 0.2$ K at $T = 2$ K. The resulting temperature gradient is perpendicular to the sample plane, which drives spin excitations from the GGG into the Pt detector, where a voltage develops as a result of the inverse spin Hall effect (ISHE). Figure 1(b) depicts the structure of the fabricated SSE device. Using these devices, our measurement results agree with the original SSE experiments on GGG [6] which were carried out at higher temperatures ($T > 5$ K), well outside of the spin-liquid regime ($T \sim |\theta_{CW}|$). Shown in Fig. 2(a) are the SSE signals measured at different temperatures with the magnetic field applied along the [100] crystal axis. The initial rise of SSE response with magnetic field is due to the increase of magnetization of GGG until almost saturation. However, we observe an appreciable downturn in the SSE response at lower temperatures in the high-field range, as can be seen in the $T = 2$ K data. This downturn is presumably caused by the opening of a Zeeman gap in the magnon spectrum [29], similar to the observation in the ferrimagnetic insulator YIG [30–32].

As described above, GGG is not simply a paramagnet. It possesses strong geometric frustration due to antiferromagnetic and dipolar interactions on the hyperkagome lattice. If one considers only the nearest-neighbor antiferromagnetic exchange interaction J, it has been shown that for a hyperkagome lattice a magnetic field with an energy scale equal to $6J$ or about 17 kOe is required to align the spins in GGG even at $T = 0$ K [33]. Our SSE experiment reflects this effect such that the maximum signal (around magnetization saturation) occurs at fields much higher than the value inferred by a Brillouin function for a noninteracting paramagnet at the same temperature [29]. We note that (as will be discussed later) because of the large dipolar interactions, the magnetic moments in GGG are in fact not fully aligned even at fields beyond 17 kOe.

Upon closer examination, the SSE signals shown in Fig. 2(a) are found not to be smooth functions of the magnetic field, but contain considerable field-dependent modulations on top of the S-shaped curve, which can be seen clearly in the derivative of the SSE signal with respect to magnetic field as shown in Fig. 2(b). In calculating the derivatives, the raw data in Fig. 2(a) were smoothened using the cubic B-spline method. From Fig. 2(b), we see that the magnitude of the modulation increases as temperature is lowered, and the modulations persist to high magnetic fields up to 90 kOe. In order to get direct information on the magnitude of the spin current modulation, we subtract a linear background in the field range -35 kOe $< H <$ 35 kOe from the SSE signal [dashed line in Fig. 2(a) [29]]. The results are shown in Figs. 2(c) and 2(d), for $T = 2$ and 3 K, respectively. When the same experiment is performed on a single-crystal YIG sample in the same temperature and magnetic field range, the modulations are absent [29]. We also rule out the possibility of magnetic-field-induced thermal conductivity or heat capacity changes as a possible source for

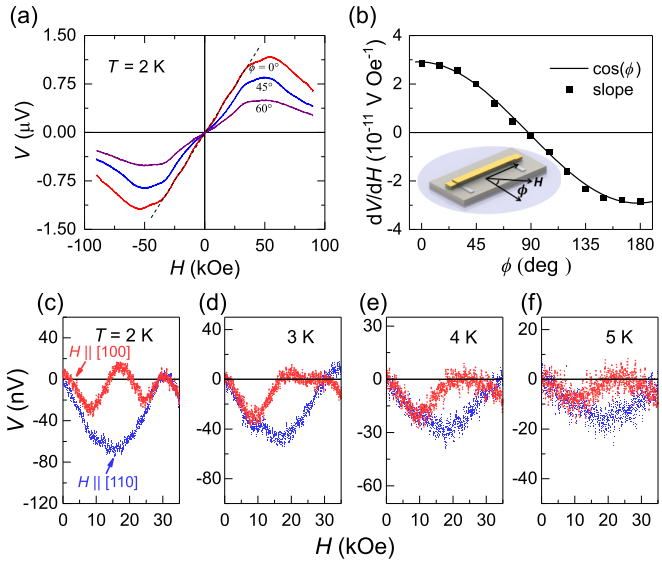

FIG. 3. Anisotropic behavior of the modulation in SSE response. (a) SSE signals measured with magnetic field applied along different directions in the (001) plane, with $\phi = 0^\circ$ being along the [100] crystal axis. (b) Magnitude of the slope of the linear part of the SSE signal satisfies cosine angular dependence. The inset shows the corresponding measurement geometry. H is the applied in-plane magnetic field. (c)–(f) Modulations in SSE voltage from $T = 2$ to 5 K. Data in red and blue correspond to field applied along the [100] and [110] directions, respectively. Notice that the modulation in SSE signal can be resolved at temperatures up to 5 K. In these measurements, the SSE devices were fabricated on the (001) surface of GGG single crystals.

this effect by independently measuring these quantities as a function of applied magnetic field [29].

Previously, neutron scattering studies on GGG found that short-range correlations persist to relatively high temperatures ($T \sim 3$ K, which is in our measurement range) [23,34]. However, little is known about their behavior in a magnetic field. For instance, are there magnetic-field-induced SROs arising in this temperature range, similar to the LROs observed at much lower temperatures? If so, the dynamics of thermally excited magnons will depend on these short-range correlations, which in turn can influence the SSE signal. It was also observed in neutron scattering and bulk magnetometry measurements that the field-induced magnetic orderings in GGG have distinct anisotropies. For instance, the critical field at which an AFM phase emerges [24,35,36] depends on the direction of the field relative to the GGG crystal axis, being different for fields aligned along the [100] versus along the [110] crystal axis [24,37]. Such anisotropy is presumably caused by dipolar interactions among Gd ions [38]. The Gd^{3+} ion in GGG carries a relatively large magnetic moment of $7\mu_B$, leading to dipolar interactions with an energy scale comparable to the nearest-neighbor exchange interaction.

To find out whether the modulation in the SSE is a probe of field-induced magnetic orderings, we performed the SSE measurements with magnetic field applied along several different GGG crystal axes. The measured SSE signals from the same device are shown in Fig. 3(a), with 0° and 45° corresponding to the [100] and [110] crystal axes, respectively. Figure 3(b) shows the overall magnitude of the SSE signal, represented by the slope of the linear background at low fields, as a function of the in-plane angle of the magnetic field. The data are fit well by a cosine function which is expected from the geometry of the ISHE, and implies that the linear background is isotropic in magnetic properties with respect to the direction of the magnetic field. In Figs. 3(c)–3(f), the modulations in the SSE signal are presented for temperatures from 2 to 5 K. In these plots, red and blue data correspond to fields applied along the [100] and [110] GGG crystal axes, respectively. For clarity, only data for the positive field range are shown. The magnitude of these modulations becomes smaller as temperature increases. At each temperature, the magnetic field dependences of the modulation are clearly different between the two field orientations. For instance, in Fig. 3(c), when the field is applied along the [100] direction, the modulation initially decreases with magnetic field and reaches a minimum at $H \sim 8$ kOe, while the minimum for the field parallel to the [110] direction occurs at $H \sim 17$ kOe. This same trend is observed at higher temperatures up to 5 K. At $T = 2$ K, however, there is a second minimum at a higher field $H \sim 24.5$ kOe for fields along the [100] direction, which is suppressed at $T > 3$ K, suggesting that this may correspond to a different order parameter than the other modulations occurring at lower fields.

Magnetic ordering in GGG has been extensively studied over the last two decades. We present a summary of these results in the Supplemental Material [29]. Upon application of a magnetic field there are FM, AFM, and incommensurate AFM phases that emerge in GGG. Most of the AFM orderings, including all incommensurate ones, have a strong temperature dependence, and they are suppressed at $T > 400$ mK [24]. However, of particular interest is the [002] AFM order, whose intensity is observable up to 900 mK [35,36], above which published experimental data are lacking. The Supplemental Material shows neutron scattering measurements at $T = 1.3$ K [29], where no scattering peak of the [002] AFM order can be resolved from the broad diffuse background. In Fig. 4, we present a direct comparison between the modulation in the SSE response at $T = 3$ K and the intensity of magnetic ordering measured by neutron diffraction at $T < 0.25$ K. Shown in Fig. 4(a) (purple data points, reproduced from Ref. [35]) are the integrated intensity of the [002] AFM peak measured by neutron diffraction as a function of magnetic field for $H \parallel [100]$. We see that the maximum position of the neutron scattering data matches the field, indicated by the vertical dashed line, where the modulation in SSE voltage shows a minimum. Crucially, for $H \parallel [110]$, the [002] AFM order from neutron diffraction reaches its maximum at $H \sim 16.7$ kOe as shown in Fig. 4(b) (reproduced from Ref. [36]), which is also in good agreement with the corresponding minimum in SSE measurements. Additionally, a small inflection in the SSE data for $H \parallel [110]$ can be seen at $H \sim 7.7$ kOe, that is also present in the neutron diffraction result. Over the entire temperature range available, the peak positions in neutron scattering data and the minima of our SSE modulations show little temperature dependence. Any remaining discrepancies may be due to the nonuniform crystal shape in the neutron scattering experiments where the demagnetization field is not considered. These comparisons provide strong evidence that

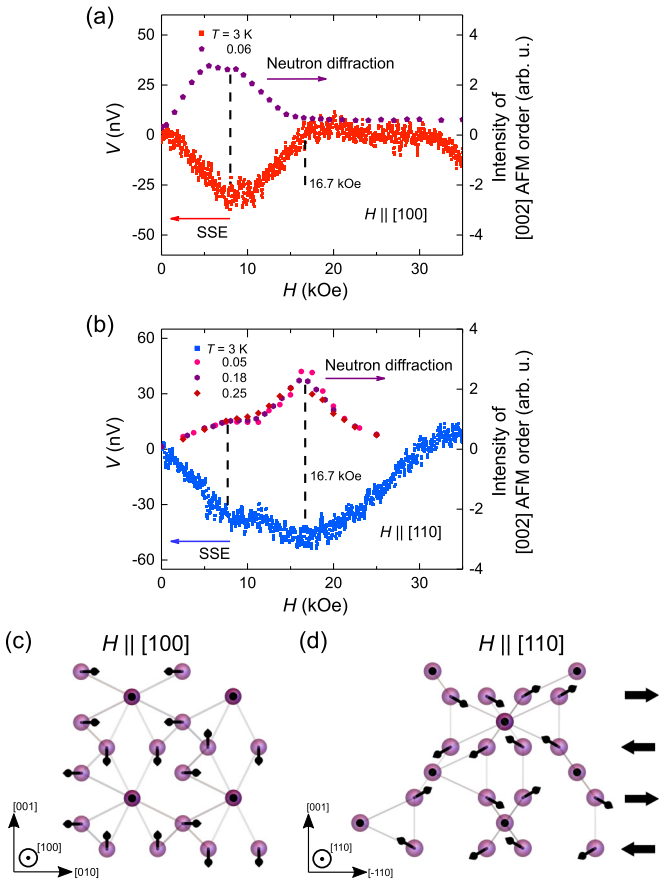

FIG. 4. Comparison between the SSE response and intensity of the [002] AFM order, and theoretical calculation of the spin configurations. (a) and (b) Magnetic field dependencies of the modulation in the SSE signal and the intensity of [002] AFM order measured by neutron diffraction with corresponding fields applied along the [100] and [110] crystal axes, respectively. Vertical dashed lines in both (a) and (b) indicate the same peak positions in the SSE data and neutron diffraction results. (c) and (d) Calculated spin configurations in one GGG primitive cell at an applied field $H = 17$ kOe aligned along the [100] and [110] crystal axes, respectively. The magnetic field points out of the page, and the spin orientation of Gd^{3+} ions is represented by a small arrow at each Gd site. Notice that most spins are canted away from the applied field. In (c) the net spin components in horizontal direction are zero, while the total horizontal components in (d), indicated by large arrows on the right, form an alternating AFM pattern with [002] wave vector.

the modulation observed in the SSE measurement is a direct probe of the [002] AFM order. Since the temperatures used in our SSE measurement are much higher than that for the disappearance of LRO peaks as measured in neutron scattering experiments [24,29], the detected magnetic ordering by the SSE is short range in character. Importantly, as shown in Fig. 4(f), the SSE can detect the SRO at temperatures up to 5 K, much higher than that for neutron scattering measurements.

The robustness of the [002] AFM order observed in our SSE measurement is striking. In order to understand its nature and its anisotropic response to magnetic fields, we have computed the spin order in GGG in the presence of a magnetic field using a Hamiltonian including exchange (J) and dipolar (D) interactions,

$$H = \sum_{j\alpha,l\beta} J_{j\alpha,l\beta}\mathbf{S}_{j\alpha}\cdot\mathbf{S}_{l\beta} - g\mu_B H\sum_{j\alpha} S^z_{j\alpha} + D\sum_{j\alpha,l\beta}\left(\frac{\mathbf{S}_{j\alpha}\cdot\mathbf{S}_{l\beta} - 3(\mathbf{S}_{j\alpha}\cdot\hat{r}_{j\alpha l\beta})(\mathbf{S}_{l\beta}\cdot\hat{r}_{j\alpha l\beta})}{r^3_{j\alpha l\beta}}\right), \quad (1)$$

where vectors $\mathbf{S}$ represent the spins at each Gd site with indices j, l identifying the unit cell, and α, β indicating the 12 Gd ions in the primitive cell, respectively. The second term in the Hamiltonian comes from the applied magnetic field H, with g and μ_B being the g-factor of Gd ions and the Bohr magneton, respectively. The vectors $\hat{r}$ denote unit vectors along the direction from site $j\alpha$ to site $l\beta$. Detailed explanations of the interaction strengths and calculation procedure are presented in the Supplemental Material [29]. An example of the calculated spin configurations are shown in Figs. 4(c) and 4(d), with $H = 17$ kOe applied along the [100] and [110] GGG crystal axes, respectively. In each graph, the perspective is chosen such that the magnetic field points out of the page. In both cases, spins at most of the Gd sites are canted away (showing transverse components) from the applied field as a result of the exchange and dipolar interactions. At $H \sim 17$ kOe, the modulation in the SSE signal is almost zero for the field along [100] [Fig. 4(a)], while its magnitude becomes largest for the field along [110] [Fig. 4(b)]. Correspondingly, our calculation of the spin configuration shows that the spin orderings are different between the two cases. For the field along [110], we find that the canting of spins leads to a net magnetization within each layer [Fig. 4(d)], with AFM ordering between layers at the [002] wave vector, as is also observed in neutron scattering measurements. In contrast, when the same field is applied along [100] [Fig. 4(c)], no AFM order develops—consistent with measurements.

In general, the SSE is associated with two effects, the magnetization carried by thermally excited magnons and their diffusivity. According to our calculation, the total magnetization of GGG at $H = 17$ kOe, taking into account the canting of spins, is very similar for the two field directions. This suggests that the large isotropic "background" SSE signal originates from excitations derived from the total magnetization. In contrast, the pattern of the canting of spins is anisotropic with the direction of the field. This suggests that the modulation in SSE signal (decrease in voltage) could be due to the decrease in the number of magnons excited, since the AFM ordering may lead to a gap in the spin-wave excitation spectrum [39] or due to reduced diffusivity arising from changes in the spin-wave dispersion due to AFM ordering. Furthermore, we show that there are modulations in the SSE response at higher fields up to 90 kOe [more clearly seen at $T = 2$ K in Fig. 2(b)]. We have not found a correspondence between those high-field modulations and existing neutron scattering measurements. Part of the reason is that currently there are very few neutron scattering studies on GGG beyond 35 kOe. Those high-field modulations revealed by the SSE may point to different spin dynamics or changes in the short-ranged magnon spectra within the material that are unique to geometrically frustrated magnets.

In conclusion, we have demonstrated that the spin Seebeck effect, in addition to serving as a generator of spin current for

spintronics applications, can also be used as a technique to probe magnetic short-range order in geometrically frustrated magnets. We find a definitive relationship between features in our SSE measurements and magnetic SRO. For gadolinium gallium garnet, our SSE measurements and comparisons to neutron scattering have revealed a *specific* field-induced AFM order from which the SRO detected by SSE is derived. The SSE signal from this SRO persists to temperatures up to 5 K, approximately five times higher than the temperature (< 0.9 K) at which neutron scattering can resolve a magnetic peak for this ordering. Furthermore, at higher magnetic fields, up to 90 kOe, our SSE measurements reveal additional structures, pointing to different spin dynamics in GGG. This approach, where we use the SSE to probe magnetic structures in the absence of long-range order, opens the door to exploring frustrated quantum magnetic systems, including samples with limited volume such as exfoliated materials and thin films. This would allow us to probe collective excitations that are only short ranged in nature, and thus largely hidden to the community, and serve as a guide for comprehensive neutron or x-ray scattering experiments.

We acknowledge very valuable discussions with Oleg Petrenko and thank him for sharing neutron data on GGG. All work at Argonne was supported by the US Department of Energy, Office of Science, Basic Energy Sciences, Materials Sciences and Engineering Division. The use of facilities at the Center for Nanoscale Materials, an Office of Science user facility, was supported by the US Department of Energy, Basic Energy Sciences under Contract No. DE-AC02-06CH11357.

C.L. and S.M.W. contributed equally to this work.

[1] G. E. W. Bauer, E. Saitoh, and B. J. van Wees, Nat. Mater. **11**, 391 (2012).
[2] K.-i. Uchida, H. Adachi, T. Ota, H. Nakayama, S. Maekawa, and E. Saitoh, Appl. Phys. Lett. **97**, 172505 (2010).
[3] S. M. Wu, W. Zhang, Amit KC, P. Borisov, J. E. Pearson, J. S. Jiang, D. Lederman, A. Hoffmann, and A. Bhattacharya, Phys. Rev. Lett. **116**, 097204 (2016).
[4] S. Seki, T. Ideue, M. Kubota, Y. Kozuka, R. Takagi, M. Nakamura, Y. Kaneko, M. Kawasaki, and Y. Tokura, Phys. Rev. Lett. **115**, 266601 (2015).
[5] Y. Shiomi and E. Saitoh, Phys. Rev. Lett. **113**, 266602 (2014).
[6] S. M. Wu, J. E. Pearson, and A. Bhattacharya, Phys. Rev. Lett. **114**, 186602 (2015).
[7] A. Aqeel, N. Vlietstra, J. A. Heuver, G. E. W. Bauer, B. Noheda, B. J. van Wees, and T. T. M. Palstra, Phys. Rev. B **92**, 224410 (2015).
[8] F. Mila, D. Poilblanc, and C. Bruder, Phys. Rev. B **43**, 7891 (1991).
[9] R. Doubble, S. M. Hayden, P. Dai, H. A. Mook, J. R. Thompson, and C. D. Frost, Phys. Rev. Lett. **105**, 027207 (2010).
[10] S. Okamoto, Phys. Rev. B **93**, 064421 (2016).
[11] H. J. Qin, K. Zakeri, A. Ernst, and J. Kirschner, Phys. Rev. Lett. **118**, 127203 (2017).
[12] J. Xiao, G. E. W. Bauer, K.-c. Uchida, E. Saitoh, and S. Maekawa, Phys. Rev. B **81**, 214418 (2010).
[13] H. Adachi, K. ichi Uchida, E. Saitoh, and S. Maekawa, Rep. Prog. Phys. **76**, 036501 (2013).
[14] S. Rezende, R. Rodríguez-Suárez, R. Cunha, J. L. Ortiz, and A. Azevedo, J. Magn. Magn. Mater. **400**, 171 (2016).
[15] S. M. Rezende, R. L. Rodríguez-Suárez, and A. Azevedo, Phys. Rev. B **93**, 014425 (2016).
[16] A. Kehlberger, U. Ritzmann, D. Hinzke, E.-J. Guo, J. Cramer, G. Jakob, M. C. Onbasli, D. H. Kim, C. A. Ross, M. B. Jungfleisch, B. Hillebrands, U. Nowak, and M. Kläui, Phys. Rev. Lett. **115**, 096602 (2015).
[17] K.-i. Uchida, T. Kikkawa, A. Miura, J. Shiomi, and E. Saitoh, Phys. Rev. X **4**, 041023 (2014).
[18] E.-J. Guo, J. Cramer, A. Kehlberger, C. A. Ferguson, D. A. MacLaren, G. Jakob, and M. Kläui, Phys. Rev. X **6**, 031012 (2016).
[19] J. Kimling, G.-M. Choi, J. T. Brangham, T. Matalla-Wagner, T. Huebner, T. Kuschel, F. Yang, and D. G. Cahill, Phys. Rev. Lett. **118**, 057201 (2017).
[20] P. Schiffer, A. P. Ramirez, D. A. Huse, and A. J. Valentino, Phys. Rev. Lett. **73**, 2500 (1994).
[21] Y. K. Tsui, C. A. Burns, J. Snyder, and P. Schiffer, Phys. Rev. Lett. **82**, 3532 (1999).
[22] J. A. M. Paddison, H. Jacobsen, O. A. Petrenko, M. T. Fernández-Díaz, P. P. Deen, and A. L. Goodwin, Science **350**, 179 (2015).
[23] O. A. Petrenko, C. Ritter, M. Yethiraj, and D. McK Paul, Phys. Rev. Lett. **80**, 4570 (1998).
[24] P. P. Deen, O. Florea, E. Lhotel, and H. Jacobsen, Phys. Rev. B **91**, 014419 (2015).
[25] W. I. Kinney and W. P. Wolf, J. Appl. Phys. **50**, 2115 (1979).
[26] S. R. Dunsiger, J. S. Gardner, J. A. Chakhalian, A. L. Cornelius, M. Jaime, R. F. Kiefl, R. Movshovich, W. A. MacFarlane, R. I. Miller, J. E. Sonier, and B. D. Gaulin, Phys. Rev. Lett. **85**, 3504 (2000).
[27] S. Ghosh, T. F. Rosenbaum, and G. Aeppli, Phys. Rev. Lett. **101**, 157205 (2008).
[28] B. Daudin, R. Lagnier, and B. Salce, J. Magn. Magn. Mater. **27**, 315 (1982).
[29] See Supplemental Material at http://link.aps.org/supplemental/10.1103/PhysRevB.98.060415 for supplemental figures, table, notes, materials, and methods.
[30] H. Jin, S. R. Boona, Z. Yang, R. C. Myers, and J. P. Heremans, Phys. Rev. B **92**, 054436 (2015).
[31] T. Kikkawa, K.-i. Uchida, S. Daimon, Z. Qiu, Y. Shiomi, and E. Saitoh, Phys. Rev. B **92**, 064413 (2015).
[32] U. Ritzmann, D. Hinzke, A. Kehlberger, E.-J. Guo, M. Kläui, and U. Nowak, Phys. Rev. B **92**, 174411 (2015).
[33] M. E. Zhitomirsky, A. Honecker, and O. A. Petrenko, Phys. Rev. Lett. **85**, 3269 (2000).
[34] O. A. Petrenko and D. McK. Paul, Phys. Rev. B **63**, 024409 (2000).
[35] O. Petrenko, G. Balakrishnan, D. McK. Paul, M. Yethiraj, and J. Klenke, Appl. Phys. A **74**, s760 (2002).

[36] O. A. Petrenko, G. Balakrishnan, D. McK. Paul, M. Yethiraj, G. J. McIntyre, and A. S. Wills, J. Phys.: Conf. Ser. **145**, 012026 (2009).

[37] A. Rousseau, J.-M. Parent, and J. A. Quilliam, Phys. Rev. B **96**, 060411 (2017).

[38] N. d'Ambrumenil, O. A. Petrenko, H. Mutka, and P. P. Deen, Phys. Rev. Lett. **114**, 227203 (2015).

[39] J. A. Quilliam, K. A. Ross, A. G. Del Maestro, M. J. P. Gingras, L. R. Corruccini, and J. B. Kycia, Phys. Rev. Lett. **99**, 097201 (2007).